



Storm dust source fingerprinting for different particle size fractions using colour and magnetic susceptibility and a Bayesian un-mixing model

Kazem Nosrati¹ · Mojtaba Akbari-Mahdiabad¹ · Shamsollah Ayoubi² · Emilie Degos³ · Axel Koubansky³ · Quentin Coquatrix³ · Simon Pulley³ · Adrian L. Collins³

Received: 28 February 2020 / Accepted: 11 May 2020 / Published online: 3 June 2020
© Springer-Verlag GmbH Germany, part of Springer Nature 2020

Abstract

In the context of the continued increased global uptake of fingerprinting procedures to explore fluvial sediment sources, far less attention has been paid to dust source tracing and especially using different particle size fractions and low-cost tracers such as colour and magnetic susceptibility. The objective of this study, therefore, was to apportion local dust storm source contributions for the < 63- μm and 63–125- μm fractions of dust samples in a case study in central Iran. Colour and magnetic susceptibility properties were measured on 62 source samples and six dust storm samples. Statistical methods were used to select four different composite fingerprints for discriminating the dust sediment sources. These statistical approaches comprised (1) the Kruskal–Wallis H test (KW-H), (2) a combination of KW-H and discriminant function analysis (DFA), (3) a combination of KW-H and principal components and classification analysis (PCCA), and (4) a combination of KW-H and a general classification and regression tree model (GCRTM). Local dust source contributions were ascribed using a Bayesian un-mixing model using the final composite fingerprints. For both the < 63- and 63–125- μm fractions, the different composite signatures consistently suggested that alluvial fan material was the dominant source of the dust samples. The root mean square differences between the apportionment results using the different fingerprints ranged from 0.5 to 1.6% for the < 63- μm fraction and from 1.8 to 5.8% for the 63–125- μm fraction. The Wald-Wolfowitz runs test was used to compare the posterior distributions of the predicted source proportions created using the alternative final composite fingerprints and the results indicated that most of the pairwise comparisons were significantly different ($p \leq 0.05$). For the < 63- μm fraction, the RMSE and MAE estimates of divergence between the modelled and known virtual source mixtures using the different final composite signatures ranged between 1.5 and 23.4% (with a corresponding mean value of 9.4%). The equivalent estimates for the 63–125- μm fraction were 1.2–20.1% (8.3%). The findings clearly demonstrate that colour and magnetic susceptibility tracers offer low-cost options for apportioning dust sources.

Keywords Modified MixSIR Bayesian model · Dust storm tracing · Statistical techniques · Alluvial fans · Aeolian sediments

Introduction

The total annual rate of storm dust mobilisation on arable land by wind erosion has been estimated to be $\sim 2 \text{ Gt year}^{-1}$ and approximately 40% of the Earth's surface (~ 4.3 million km^2 of dry-land) (Ravi et al. 2011) is prone to erosion by wind (Thomas and Middleton 1997). In a review of the dust cycle as an emerging phenomenon, Shao et al. (2011) included the results of 13 studies that estimated total global dust emissions to be in the range of 500 to $\sim 3320 \text{ Tg year}^{-1}$. Storm dust is therefore a global environmental problem worthy of attention.

Responsible Editor: Philippe Garrigues

✉ Kazem Nosrati
k_nosrati@sbu.ac.ir

¹ Department of Physical Geography, School of Earth Sciences, Shahid Beheshti University, Tehran 1983969411, Iran

² Department of Soil Science, College of Agriculture, Isfahan University of Technology, Isfahan 8415683111, Iran

³ Sustainable Agriculture Sciences Department, Rothamsted Research, North Wyke, Okehampton EX20 2SB, UK

More than two-thirds of Iran's land area is subject to arid and semi-arid climates with deserts covering approximately 20% of the area. Wind erosion has been estimated to be affecting ~ 20 million hectares of land (NAP 2005). Storm dust phenomena occur frequently in Iran. The average dust storm days has been reported to vary between 23 and 80 days per year (Middleton 1986). The socioeconomic impacts of storm dust include compromising visibility, health problems (especially ophthalmic and respiratory diseases), and soil loss from crop land fields (Al-Hemoud et al. 2019; Reheis 2006). Information on storm dust provenance is therefore an important requirement for developing targeted abatement strategies. The results of a study based on remote sensing techniques by Prospero et al. (2002) showed that the dominant dust sources are alluvial materials deposited by irregular periodic flooding during the Quaternary and Holocene. In arid and semi-arid lands more generally, alluvial material is deposited during storm rainfall events, thereby providing a potential source of wind-erodible material (Ginoux et al. 2012). Protecting different environments from the invasion of aeolian sediments (sand dunes and storm dust) and associated pollutants requires techniques that can answer key questions such as which land use types or landforms are key sources of local storm dust in impacted areas? Assessment of storm dust sources is vital to educate people in impacted areas so that they can manage the dust issue which is degrading social, environmental, and economic pillars of sustainability. Therefore, there is an ongoing need for research to quantify the contributions of individual dust sources for targeting best management practices for wind erosion control.

The concept of sediment source fingerprinting was originally developed to un-mix fluvial sediments into multiple sources using different tracers. A key stage in the fingerprinting approach concerns the discrimination of potential sources and, to date, different multivariate statistical methods have been used to identify composite signatures comprising different sets of tracers (Collins et al. 2012; Nosrati and Collins 2019a; Nosrati and Collins 2019b; Nosrati et al. 2018; Palazón et al. 2015; Palazón and Navas 2017; Pulley et al. 2017; Tiecher et al. 2015).

Applications of the fingerprinting approach to assess aeolian sediment provenance using alternative composite signatures have recently (since 2016) started emerging in the international literature, but these studies focus on sand dune sediment rather than storm dust. More recently (2019 to 2020), two papers were published in the specific case of source fingerprinting atmospheric dust using GLUE and Monte Carlo simulation (Behrooz et al. 2019; Gholami et al. 2020). In recognition of the latter gap in current applications of the fingerprinting approach and the need for further work, we tested colour and magnetic susceptibility properties for tracing storm dust origin using Bayesian un-mixing model. Magnetic susceptibility measurements have been widely used in several fields (Asgari et al. 2018; Bourliva et al. 2018; Caitcheon

1993; Karimi et al. 2013, 2017; Mathé and Lévêque 2003; Morris et al. 1994; Shenggaio 2000; Valaee et al. 2016), but not for tracing storm dust sources. The same is true of colour, since previous work has used colourimetric properties to investigate fluvial sediment sources (e.g. Martínez-Carreras et al. 2010). Existing studies applying sediment source fingerprinting to estimate sand dune and storm dust provenance have primarily used elemental geochemistry (e.g. Behrooz et al. 2019; Gholami et al. 2019a; Gholami et al. 2017, 2019b, 2020; Liu et al. 2016; Muhs and Budahn 2019) and end-users therefore need evidence of the potential utility of alternative types of tracers for understanding the source dynamics of aeolian sediment. Dust storms in the Bahadoran region study area started ~ 10 years ago due to droughts, groundwater scarcity, vegetation loss, and land use change. The on-site and off-site effects of storm dust in the study area comprise soil loss from crop lands, decreasing agricultural production, and reductions in land utility compromised visibility, as well as health problems. Assembling reliable evidence for targeting abatement measures is therefore a local policy priority. On this basis, the objective of this study was to apportion local source contributions to the < 63- and 63–125- μm fractions of dust samples in a case study in central Iran using colour and magnetic properties in conjunction with a Bayesian un-mixing model. We tested colour and magnetic properties since these are low cost and thereby accessible to more researchers interested in applying the fingerprinting approach to dust problems in arid and semi-arid environments.

Materials and methods

Study area

The study area, known as the Bahadoran region or plain (3345.4 km²), is located to the south-east of Mehriz city, Yazd Province, in central Iran between 54° 39' 03" to 55° 20' 46" E longitude and 30° 39' 33" to 31° 35' 35" N latitude (Fig. 1). The Bahadoran is a small plain within the larger Yazd-Ardakan plain and is characterised by relatively fertile soils, considered to be one of the major agricultural and pistachio production areas in Yazd province. The topography of the study area comprises a mixture of plain, pediment, and mountain. The elevation of the study area ranges from 1334 to 2830 m above sea level. A land use map of the study area prepared by the Iran Forests, Range and Watershed Management Organization (IFRWMO) shows that the land cover includes rangelands and bushlands (2839 km² area; 84.9%), rock outcrops (374 km² area; 11.2%), agricultural lands, (105 km² area; 3.1%), aeolian sediment and sand dunes (25 km² area; 0.7%), and residential areas (2 km² area; 0.1%). The principal lithology comprises marl, sandy marl, red and green (E_m), andesite to trachy andesite (E_v), granite to granodiorite (Dogger) (g^{sh}),

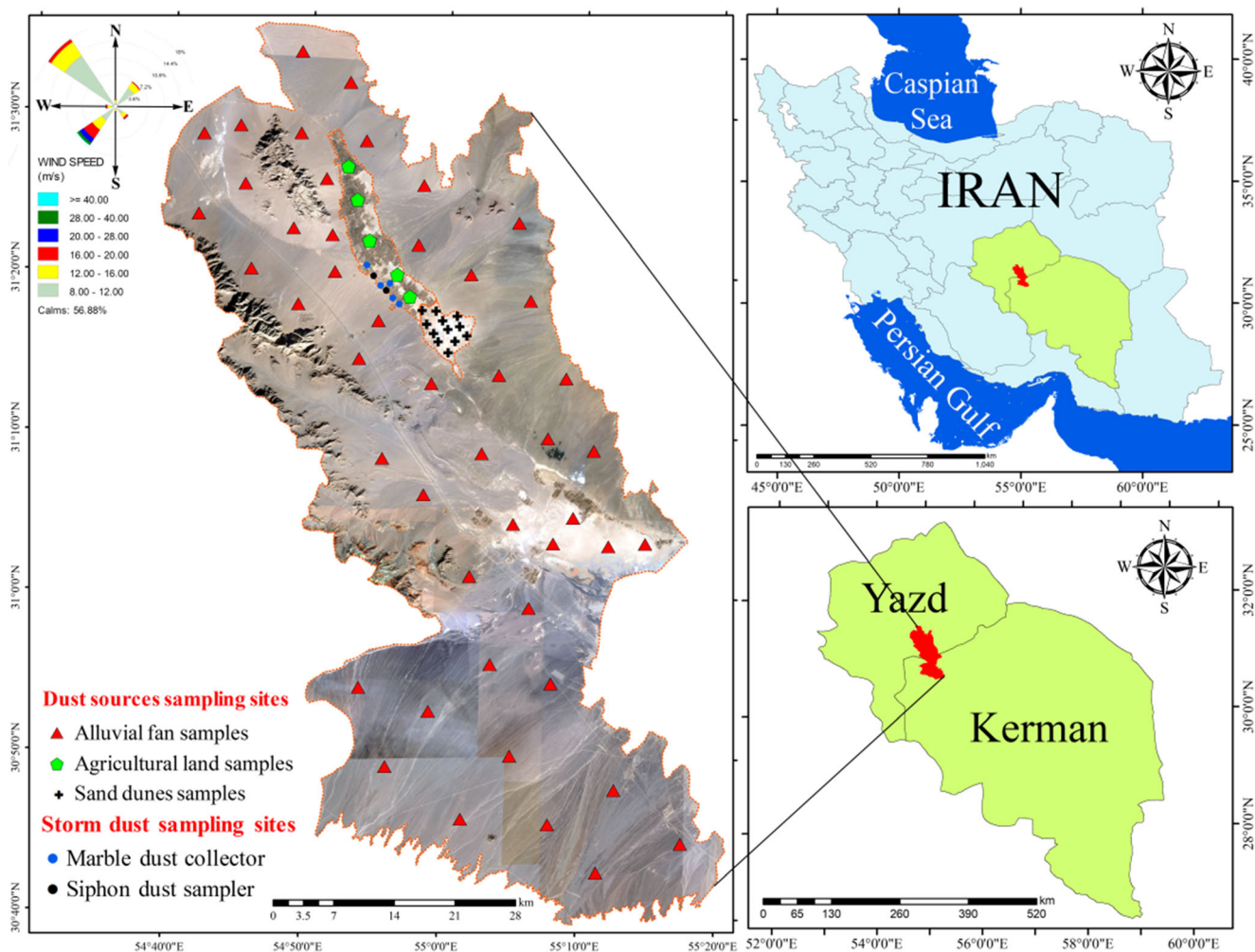


Fig. 1 Map of the study area in Yazd Province, central Iran, storm dust sampling locations and source sampling sites

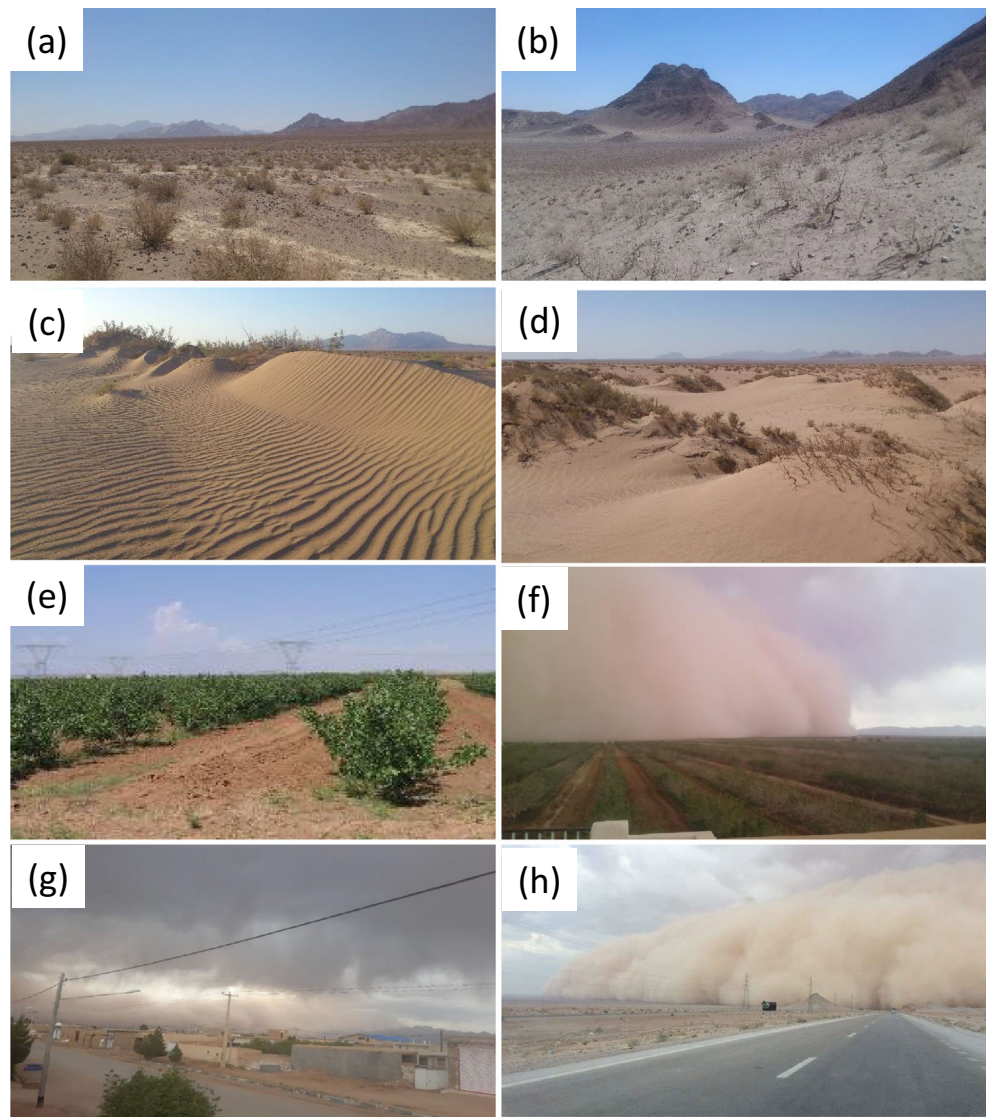
marl, shale (K_{dz}), sandstone, conglomerate, red (K_s), limestone partly marmorised (K_l), grey, thick to massive, cliff forming orbitolina limestone (K_{t3-1}), upper limestone (K_{uy}), red beds, sandstone, sand marl, conglomerate (E_1^{tsh}), upper conglomerate (N_{g2}), conglomerate, poorly consolidated (N_{g2c}), hornblende-pyroxene andesite (N_{g2a}), Kerman conglomerate (P_{gk}), Jamal type limestone (P_j), low-level pediment fan and valley terrace deposits (Q_{f2}), and salt flat (Q_{sf}). The soil map of Iran prepared by the IFRWMO shows that the main soil orders are Entisols and Aridisols. Using data (1986–2015) collected by the Iran Meteorological Organization at Bahadorn and Mahdiabad climatologic stations in the study area, the mean annual rainfall is ~ 70 mm. Mean monthly minimum/maximum temperatures are 12°C and 43°C , respectively. Using the De Marton climate grouping, the climate is cold arid and the study area is influenced by the warm and dry weather of the central plain of Iran, meaning that it has very hot summers and very cold winters. A wind rose is available based on a 14-year long-term wind data record (2003–2017), at Bahadorna climatological station in the study area ($54^\circ 54' 01''$ E longitude and $31^\circ 13' 13''$ N latitude).

The wind rose data suggests that the prevailing wind directions are generally north-western to south-eastern and south-western to north-eastern. The main erosive wind (with a velocity > 21 m s^{-1}) direction is also south-western to north-eastern and north-western to south-eastern (Fig. 1).

Fieldwork and laboratory analyses

Wind-rose and sand-rose diagrams were prepared to establish the main and effective wind directions as the assumption here is that the dominant dust sources are in the direction of major effective winds. Prior to sampling, reconnaissance field surveys were undertaken to identify potential key dust sources. These potential dust sources were classified as alluvial fans (Fig. 2a and b), aeolian sand dunes (Fig. 2c and d), and agricultural land (Fig. 2e and f). The target dust samples were collected during local dust storm events in the residential areas of Bahadorn village (Fig. 2g and h).

Fig. 2 Photos showing the dust sources (a and b), alluvial fans (c and d), aeolian sand dunes and agricultural land (e and f), and dust storm events (g and h)



In total, 62 dust source samples were retrieved to characterise these key sources, including 45 samples from the northern, western, southern, and eastern alluvial fans and pediment; 12 from aeolian sand dunes; and five from agricultural land (Fig. 1). In order to increase the representativeness of the source samples and to take some account of spatial variability in tracer content, each source sample represented a composite of 5 sub-samples collected within ca. 100 m² at a specific site. Here, source samples were collected from the upper 5 cm of the soil layer to represent material at risk of mobilisation and redistribution by wind erosion (Gholami et al. 2017).

All individual storm dust samples were retrieved during dust storm events using five marble dust collectors (Fig. 3a) installed at a height of 4 m and two siphon dust samplers (1.8 m height; Fig. 3b). The geographical coordinates of the marble dust collectors are presented in Fig. 1. The siphon dust samplers were installed at the Bahadoran (54° 54' 01" E longitude and 31° 13' 13" N latitude) and Mahdiabad (54° 54' 24" E

longitude and 31° 19' 54" N latitude) climatologic stations (Fig. 1). Sampling was undertaken at an approximate monthly interval at different strategic locations across Bahadoran village during six local dust storm events in 2018; 21 March, 21 April, 22 May, 22 June, 23 July, 23 August, and 23 September. Samples were composited together to provide sufficient mass for tracer laboratory analyses.

In order to determine the dominant particle size fraction by mass in the storm dust samples and to show that the tracers we used are distributed across that fraction, a two-step procedure was implemented: (1) dry sieving to separate fractions of 250–500 μm, 125–250 μm, and < 125 μm and (2) tracer analysis to confirm tracer distribution. The results of this work confirmed that the < 125-μm fraction was dominant (Fig. 3c). In the second step, all samples were fractionated into < 63 and 63–125 μm to assess whether the tracers were distributed across the < 125-μm fraction or within the sub-fraction (63–125 μm).

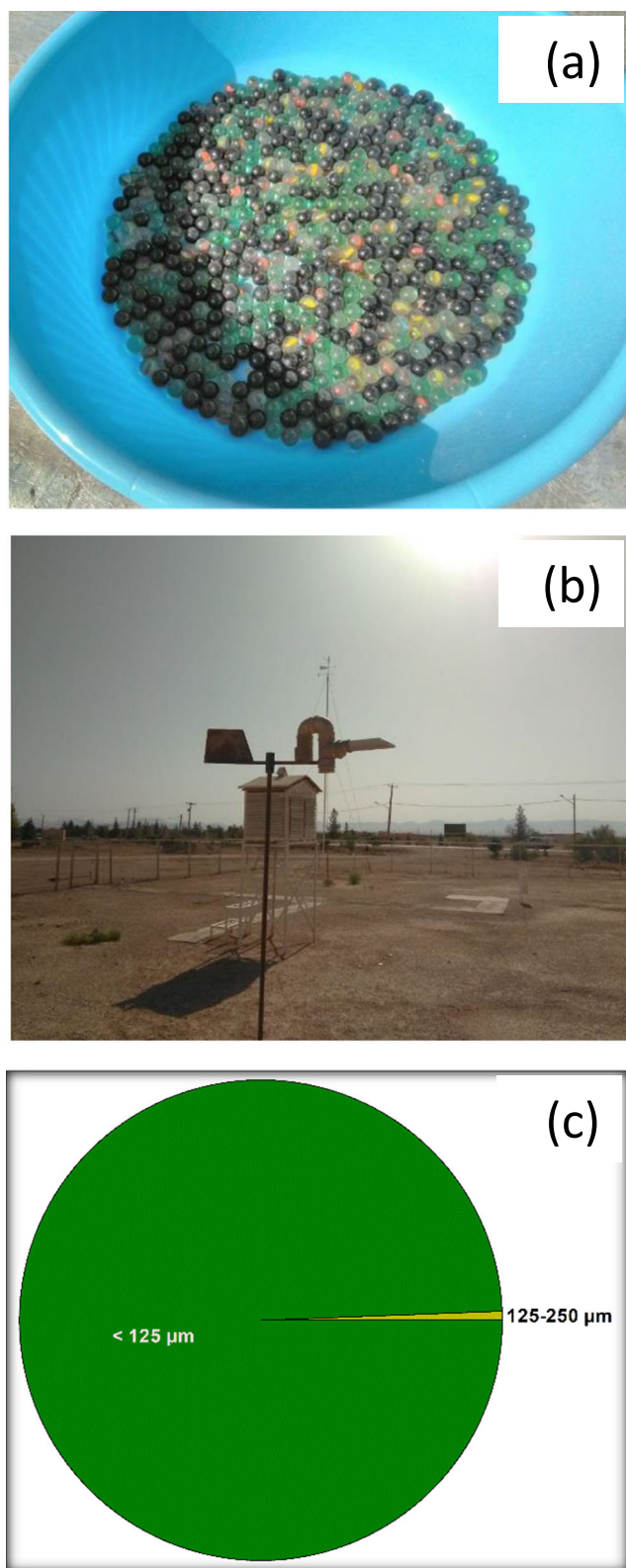


Fig. 3 **a** Marble dust collector, **b** siphon sand sampler, and **c** particle size distribution of the samples

For the colour tracers, source and target storm dust samples were placed into transparent polythene bags and

scanned using a Xerox WorkCentre 7120 colour scanner. All the generated images were processed using the GIMP 2 open-source image editing software and the RGB colour model. Here, red, green, and blue were estimated on a scale of 0 to 255.

A Bartington MS2 dual-frequency sensor was used for measurements of target storm dust and source sample magnetic susceptibility (χ) at low (0.47 kHz; χ_{lf}) and high (4.7 kHz, χ_{hf}) frequency using about 10 g of each sample which were placed in a plastic vial with a 2.3-cm diameter. Equation 1 was used to calculate the dependent frequency (χ_{fd}) (Dearing et al. 1996):

$$\chi_{fd} = [(\chi_{lf} - \chi_{hf}) / \chi_{lf}] \times 100 \quad (1)$$

Statistical discrimination of storm dust sources

Before running statistical tests to select the final sets of tracers in the composite fingerprints, conservation tests were carried out based upon the bracket or range test and biplots to identify significantly non-conservative tracers for both particle size fractions. The bracket tests (Foster and Lees 2000) were run based on two comparisons. Firstly, the minimum and maximum concentrations of each tracer measured for the dust sources were calculated and compared with the corresponding concentrations measured for the target dust samples. If a tracer for the target storm dust samples fell outside the ranges of the concentrations in the sources, that tracer was removed from further analysis. Secondly, the average tracer concentrations in the target dust samples were calculated and compared with the ranges of the average tracer concentrations for all dust sources. This second range test is considered to be stricter. Finally, after selecting the final sets of tracers for discriminating the storm dust sources, biplots of tracer concentrations in source and target storm dust samples were generated for both particle size fractions as a further and more sensitive means of assessing tracer conversion during dust transportation and deposition processes.

Statistical methods were used to select four alternative composite fingerprints for discriminating the storm dust sources. These statistical tests comprised (1) the Kruskal–Wallis H test (KW-H), (2) a combination of KW-H and discriminant function analysis (DFA), (3) a combination of KW-H and principal components and classification analysis (PCCA), and (4) a combination of KW-H and a general classification and regression tree model (GCRTM). Further details on these tests can be found in Nosrati and Collins (2019a), Nosrati and Collins (2019b) Nosrati et al. (2018), and Nosrati et al. (2019). Four different composite signatures were selected using these tests which were applied using STATISTICA V.8.0 (StatSoft 2008).

Table 1 Tracer concentration data for the < 63- and 63–125- μm fractions for the sources and target dust samples and the Kruskal–Wallis H test results for discriminating the individual dust sources. The RGB raw data reflect red, green, and blue light and are measured by base 10 (decimal) values ranging from 0 to 255

Sediment sources	Statistics	< 63- μm fraction						63–125- μm fraction					
		Red	Green	Blue	χ_{lf}^{**}	χ_{hf}	χ_{fd}	Red	Green	Blue	χ_{lf}	χ_{hf}	χ_{fd}
Alluvial fan	Mean	169.6	166.7	137.3	434.4	432.6	0.5	163.5	146.4	119.8	457.6	456.0	0.4
	SD	6.5	5.7	5.3	299.3	298.5	0.2	10.0	8.1	6.6	351.6	350.8	0.2
Sand dunes	Mean	205.7	183.9	154.1	158.4	157.1	0.9	189.6	171.7	145.4	133.2	132.4	0.7
	SD	4.5	5.0	5.3	70.4	70.4	0.3	5.5	5.9	5.8	82.7	82.7	0.4
Agricultural land	Mean	191.0	152.4	123.6	166.7	165.2	0.9	179.7	158.8	131.3	142.9	141.9	0.8
	SD	5.5	5.2	4.5	34.1	34.0	0.4	6.2	4.4	3.1	40.1	39.9	0.6
KW-H test	Chi-Square	30.4	28.8	29.1	22.4	22.6	19.5	28.4	25.7	25.8	22.4	22.6	12.1
	<i>p</i> value	< 0.001*	< 0.001*	< 0.001*	< 0.001*	< 0.001*	0.001*	< 0.001*	< 0.001*	< 0.001*	< 0.001*	< 0.001*	0.002*
Dust samples	1	176.4	159.4	131.9	232.8	231.4	0.6	155.4	139.5	114.6	220.6	219.7	0.4
	2	163.9	147.4	120.2	416.7	415.8	0.3	154.3	138.5	114.0	436.7	436.4	0.1
	3	171.4	154.8	128.4	141.2	139.2	1.4	158.7	142.8	119.7	113.0	111.4	1.4
	4	170.2	152.9	126.2	252.2	250.7	0.6	156.3	140.6	117.6	243.4	242.4	0.4
	5	174.4	154.5	127.1	306.3	304.8	0.5	167.3	149.6	123.3	307.0	305.9	0.4
	6	178.3	161.4	133.6	229.8	227.7	0.9	166.6	151.8	128.3	217.2	215.4	0.8
	Mean	172.4	155.1	127.9	263.2	261.6	0.7	159.8	143.8	119.6	256.3	255.2	0.6

*Critical *p* value = 0.05. *KW-H test*, Kruskal–Wallis H test. ** χ_{lf} , magnetic susceptibility at low frequency ($10^{-8} \text{ m}^3 \text{ kg}^{-1}$), χ_{hf} high frequency ($10^{-8} \text{ m}^3 \text{ kg}^{-1}$), and χ_{fd} dependent frequency ($10^{-8} \text{ m}^3 \text{ kg}^{-1}$)

Storm dust source apportionment

Fluvial sediment source tracing studies are increasingly using Bayesian un-mixing models (Collins et al. 2017) including Modified MixSIR for source apportionment purposes (Nosrati 2017; Nosrati and Collins 2019a; Nosrati et al. 2014, 2018). On this basis, we applied Modified MixSIR. The model was applied using three key steps (Nosrati et al., 2014) comprising (1) calculation of the prior probability distributions for model factors; (2) creation of a likelihood function for the statistical model; and (3) extraction of the posterior probability distributions for the factors using the Bayes rule to calculate the relative contributions from the sources to the target storm dust samples. For both particle size fractions, 10^6 samples were drawn from the posterior distributions of the estimated target storm dust mixtures in MATLAB using the sampling-importance-resampling (SIR) algorithm (Moore

and Semmens 2008). All of the parameters in the model are proportional contributions from each source, and they are bounded within the interval 0–1. Also, the bounded proportions sum to 1. For both particle size fractions, the two-sample Wald-Wolfowitz runs test was used to test for statistically significant differences between the distributions of the posterior proportional contributions computed for the three dust sources using each of the different composite signatures. Additionally, for both particle size fractions, predicted source proportions using the different statistical approaches were also compared using the root mean square difference.

The Modified MixSIR predictions of source proportions were evaluated using 7 sets of virtual dust mixtures for each composite signature for both particle size fractions using a range of source proportions: (1) equal proportions from each dust source—33.3% alluvial fan, 33.3% sand dunes, 33.3% agricultural land; (2) 50% alluvial fan, 25% sand dunes, 25% agricultural land; (3)

Table 2 Summary of the backward discriminant function analysis (DFA)

Function	Eigenvalue	Canonical correlation	Wilks' lambda	Chi-square	<i>p</i> -level
< 63- μm fraction					
0	3.9	0.89	0.09	140.9	< 0.0001
1	1.2	0.74	0.46	46.5	< 0.0001
63–125- μm fraction					
0	2.4	0.84	0.18	99.5	< 0.0001
1	0.7	0.63	0.60	29.6	< 0.0001

Table 3 Selected tracers by backward discriminant function analysis (DFA) and associated statistics

Tracer	Wilks' lambda	Partial lambda	F-remove	p-level	Tolerance	1-tolerance
< 63-μm fraction						
Blue	0.15	0.62	17.4	< 0.0001	0.03	0.97
Red	0.26	0.36	51.6	< 0.001	0.03	0.97
Green	0.19	0.48	31.4	< 0.0001	0.01	0.99
χ_{fd}^1	0.12	0.80	7.3	0.001	0.90	0.10
63–125-μm fraction						
Blue	0.31	0.58	20.6	< 0.0001	0.03	0.97
Red	0.39	0.46	33.1	< 0.0001	0.01	0.99
Green	0.35	0.51	27.2	< 0.0001	0.01	0.99
χ_{fd}	0.20	0.88	3.7	0.03	0.91	0.09

¹ Magnetic susceptibility dependent frequency (χ_{fd})

25% alluvial fan, 50% sand dunes, 25% agricultural land; (4) 25% alluvial fan, 25% sand dunes, 50% agricultural land; (5) 75% alluvial fan, 10% sand dunes, 15% agricultural land; (6) 15% alluvial fan, 75% sand dunes, 10% agricultural land; and (7) 10% alluvial fan, 15% sand dunes, 75% agricultural land. Since the virtual dust mixtures were constructed using the measured tracer data for the dust source samples, the tracer concentrations in the virtual mixtures satisfied the bracket tests for tracer conservation. Root mean square error (RMSE) and mean absolute error (MAE) were used to assess the accuracy of the Bayesian modelling in solving virtual sediment mixtures. This stage in the source fingerprinting procedure tests the accuracy of the predicted source proportions by comparing them with the known source proportions in the virtual mixtures.

Results and discussion

Final composite signatures

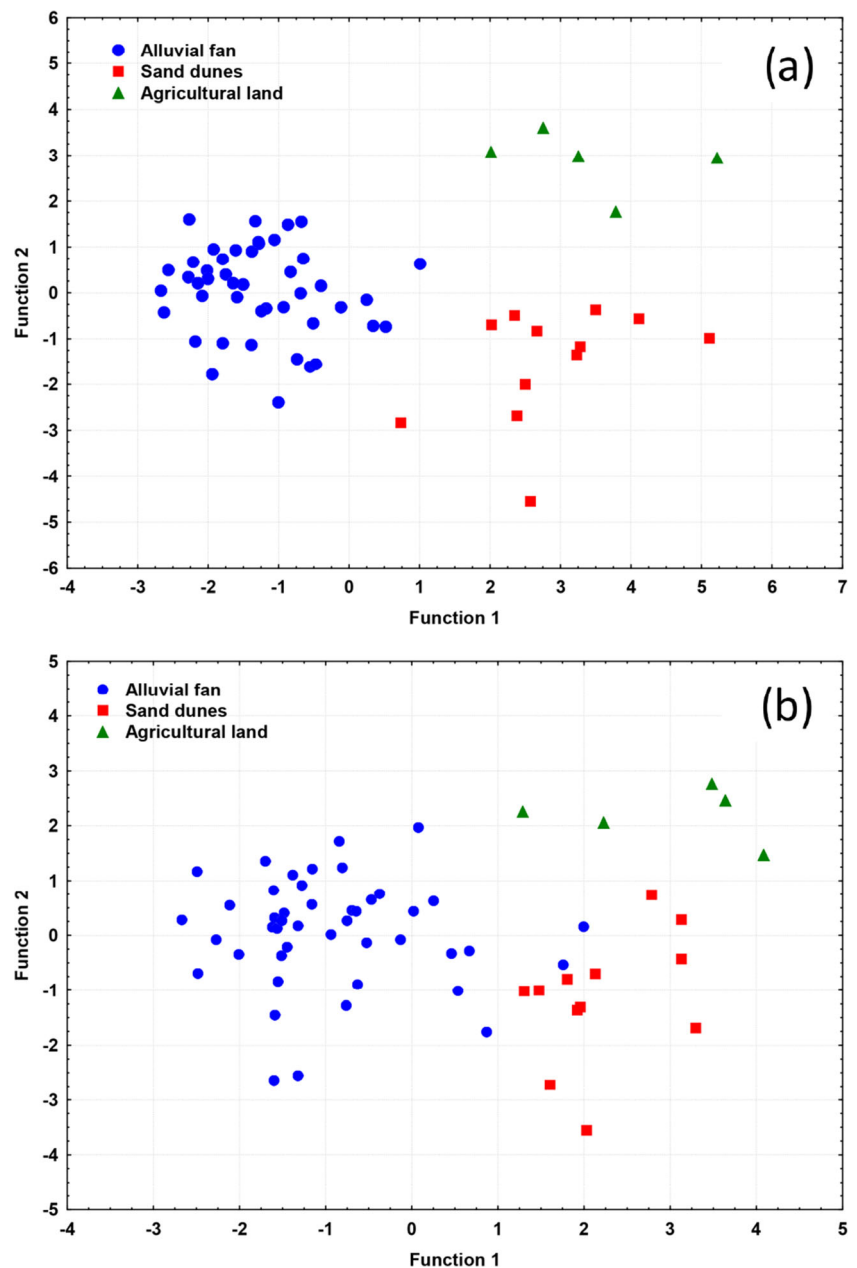
Table 1 compares the tracer concentrations in the storm dust sources and target dust samples for the < 63- and 63–125- μ m particle size fractions. The results of the bracket tests showed that all tracers (red, green, and blue colour properties, as well as magnetic susceptibility: χ_{lf} , χ_{hf} , and χ_{fd}) were broadly conservative. The KW-H test (Table 1) indicated that all tracer properties showed a statistically significant difference between the dust sources. All tracers were therefore selected as a composite signature for use in the Modified MixSIR un-mixing model for both particle size fractions.

Table 4 Summary of the backward discriminant function analysis (DFA)

Dust sources	DFA parameters	Dust sources		
		Alluvial fan	Sand dunes	Agricultural land
< 63-μm fraction				
Alluvial fan	Mahalanobis distance	0.0		
	Classified (%) correctly	100.0		
Sand dunes	Mahalanobis distance	21.9*	0.0	
	Classified (%) correctly	0.0	100.0	
Agricultural land	Mahalanobis distance	33.1*	19.6*	0.0
	Classified (%) correctly	0.0	0.0	100.0
63–125-μm fraction				
Alluvial fan	Mahalanobis distance	0.0		
	Classified (%) correctly	93.3		
Sand dunes	Mahalanobis distance	11.2*	0.0	
	Classified (%) correctly	100.0	100.0	
Agricultural land	Mahalanobis distance	19.5*	11.6*	0.0
	Classified (%) correctly	100.0	100.0	100.0

*Significant at 0.05 level

Fig. 4 Scatterplot of the first and second discriminant functions calculated using backward DFA associated with selection of the composite signature for **a** the < 63- μm fraction and **b** the 63–125- μm fraction



The six properties passing the KW-H test were then entered into the backward stepwise DFA (Table 2). For the < 63- μm fraction, the first function of the Wilks' lambda value (0.09) showed that about 99% of the total variance among the storm dust sources was explained by these six tracers. The canonical correlation values for the first and second functions were 0.89 and 0.74, respectively, indicating a strong relationship between the discriminant scores and the storm dust source groups (Table 2). The discriminatory power of the tracers in the DFA model for each particle size fraction was determined using Wilks' lambda statistics. Four tracers comprising red, green, blue, and χ_{fd} were selected based upon Wilks' lambda values for both particle size fractions (Table 3). The partial

Wilks' lambda values indicated that red contributed the most, green second most, blue third most, and χ_{fd} the least to the overall discrimination (Table 3).

The backward stepwise DFA classification results showed that 100% and 95% of the dust sources samples were grouped correctly based on the selected tracers for the < 63- and 37–63- μm particle size fractions, respectively (Table 4). The squared Mahalanobis distance statistics showed that the dust sources were strongly discriminated for both particle size fractions (Table 4). Similarly, a scatterplot of the first and second discriminant function scores computed using backward DFA demonstrated that the dust source samples were well separated for both size fractions (Fig. 4).

Table 5 Principal component and classification analysis (PCCA) factor coordinates of the variables and the eigenvalues of the correlation matrix

Tracer	PC 1	PC2	Communality estimates
<i>< 63-μm fraction</i>			
Red	<i>0.911</i>	0.36	0.96
Green	0.89	0.45	0.99
Blue	0.84	0.50	0.97
χ_{lf}	-0.72	0.67	0.95
χ_{hf}	-0.72	<i>0.67</i>	0.96
χ_{fd}	0.71	-0.28	0.58
Eigenvalue	3.9	1.6	
% Total variance	64.4	25.9	
Cumulative % variance	64.4	90.3	
<i>63–125 fraction</i>			
Red	<i>0.94</i>	0.30	0.97
Green	0.91	0.41	0.99
Blue	0.84	0.51	0.96
χ_{lf}	-0.71	0.68	0.96
χ_{hf}	-0.71	<i>0.68</i>	0.97
χ_{fd}	0.57	-0.21	0.37
Eigenvalue	3.7	1.5	
% Total variance	62.0	25.0	
Cumulative % variance	62.0	87.0	

¹ Italic values indicate selected tracers with highest loadings

Magnetic susceptibility at low frequency (χ_{lf}) and high frequency (χ_{hf}) and dependent frequency (χ_{fd})

Tracers passing the KW-H test in both particle size fractions were also tested using PCCA. The results of PCCA for the $< 63\text{-}\mu\text{m}$ fraction indicated that the first and second PCs have eigenvalues of more than one and explained more than 90% of the total variance among the tracer values for the storm dust end members (Table 5). The communality values showed that all five tracers, except χ_{fd} , have a value > 0.95 . Thus, χ_{fd} was the least significant tracer because of its lowest communality value (Table 5). The first PC, with an eigenvalue of 3.9, accounted for about 64% of the total variance among the dust end members. The second PC with an eigenvalue of 1.6 explained about 25% of the total variance (Table 5). In order to finalise tracer selection using the first PC, a threshold for the range of absolute values was set as needing to be within 10% of the highest loading. Since the red tracer has the highest loading value (0.91), the alternative tracer loadings should thereby exceed 0.82. Red, green, and blue (i.e. all colourimetric tracers) all returned loadings exceeding 0.82. In order to select tracers from the second PC, a similar approach was implemented whereby the tracer loadings needed to exceed a threshold equivalent to within 10% of the highest loading tracer (χ_{hf} with a loading of 0.671). On this basis, the tracer loadings needed to exceed 0.6. In this case, χ_{lf} and χ_{hf} (Table 5) returned loadings exceeding 0.6.

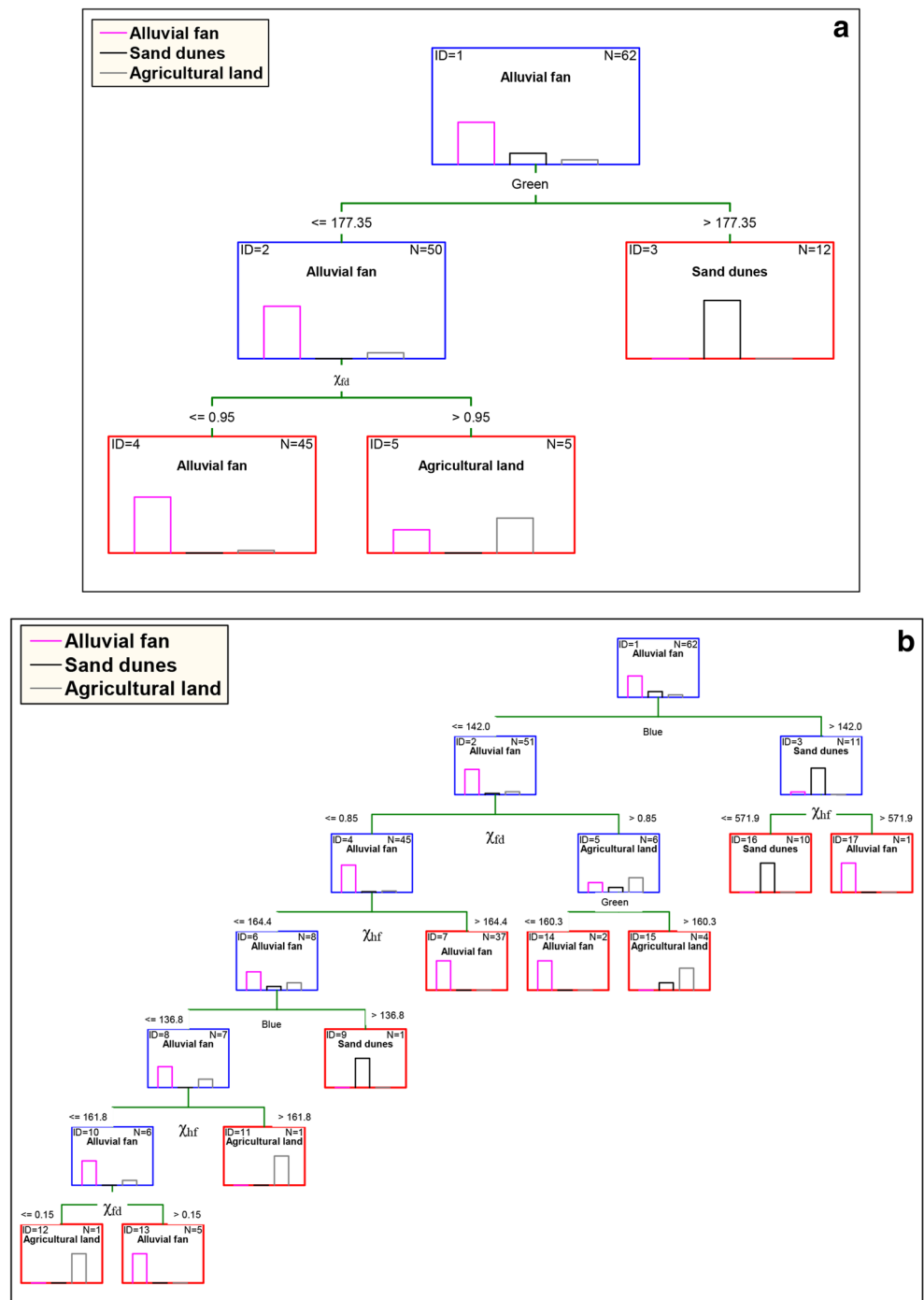
Due to correlation between these tracers, only χ_{hf} was included in the final composite signature since it returned the highest loading.

The results of the PCCA for the 63–125- μm fraction indicated that the first and second PCs have eigenvalues of more than one and explained more than 87% of the total variance among the tracer values for the storm dust end members (Table 5). All five tracers, except χ_{fd} , returned a communality value > 0.96 . The first PC, with an eigenvalue of 3.7, accounted for about 62% of the total variance among the dust end members. The second PC, with an eigenvalue of 1.5, explained about 25% of the total variance (Table 5). The red tracer returned the highest loading of 0.94 and additional tracers were retained if their loadings exceeded 0.84 (i.e. a threshold within 10% of the maximum loading). Red, green, and blue all returned loadings exceeding 0.84. Due to significant correlation issues between these tracers, red, with the highest loading, was retained for the final composite signature. A consistent approach was adopted to identify tracers from the second PC wherein χ_{hf} returned the highest loading of 0.681, meaning that the selection threshold was 0.61. χ_{lf} and χ_{hf} (Table 5) returned loadings > 0.61 , but only χ_{hf} was retained in the final composite signature for this coarser particle size fraction because these PC2 tracers were strongly correlated.

During the data mining for both particle size fractions, the six tracers passing KW-H were entered into a general classification and regression tree model (GCRTM). The final trees that were determined based on the tracers v-fold cross-validation (CV cost) test are presented in Fig. 5. For the $< 63\text{-}\mu\text{m}$ fraction, the final tree classified the dust end members into three terminal nodes (i.e. the sampled dust sources) using the cases (samples for all sources) collected to characterise these potential sources with minimum CV cost (0.09). For this finer particle size fraction, the classification results (the histograms of samples in each class at the nodes in the final tree) illustrated that 100% of the cases were classified correctly (Fig. 5a). For the 63–125- μm fraction, the final tree also classified the dust end members into three terminal nodes using the cases with minimum CV cost (0.12). Here, the classification results (the histograms of samples in the final tree) showed that 100% of the cases were also classified correctly (Fig. 5b).

The bar plots of predictor importance using dust sources as the dependent variable and the tracer variables as the predictors are shown in Fig. 6. For each tracer in this final signature, the predictor importance was calculated based on the relative average of the sum of squares of prediction for all trees and nodes for which the maximum value of predictor importance equals to 1. Hence, the predictor importance values reveal the power of the relationship between the tracers and the storm dust source of interest over the sequential boost up steps. In this case, for the $< 63\text{-}\mu\text{m}$ fraction, the tracers red, green, and blue (importance value ≥ 0.9) stand out as the most important predictors within this particular final set of tracers (Fig. 6a).

Fig. 5 The classification tree for the storm dust sources using GCRTM for **a** the < 63- μm fraction and **b** the 63–125- μm fraction



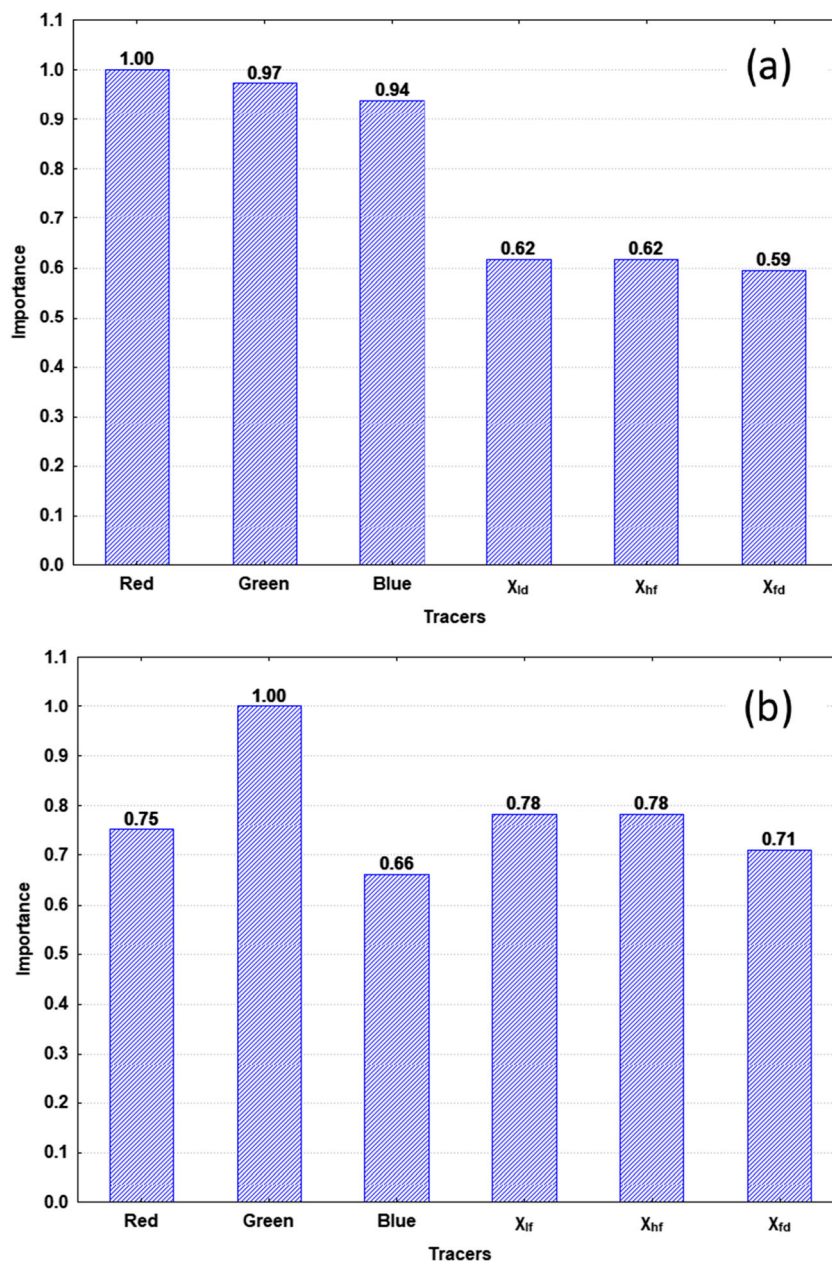
For the 63–125- μm fraction, the tracers red, green, χ_{lf} , χ_{hf} , and χ_{fd} (importance value ≥ 0.7) stand out as the most important predictors within this final set of tracers.

Using the above statistical analyses, four composite signatures were used in the Modified MixSIR un-mixing model for storm dust source apportionment. The biplots in Fig. 7 suggested that the tracers selected in the final composite signatures had not been subjected to major transformation during redistribution from the source to the target dust sampling locations.

Storm dust end member contributions

Considering priors and estimations of uncertainty associated with the un-mixing model inputs, Modified MixSIR model runs of 10^6 iterations, for each composite signature for each particle size fraction, resulted in convergence of the solutions. The maximum importance ratio values (calculated by determining the ratio of the maximum un-normalised posterior probability resample to the sum of all un-normalised posterior

Fig. 6 The importance plot of the dust sources using GCRTM for **a** the $< 63\text{-}\mu\text{m}$ fraction and **b** the $63\text{--}125\text{-}\mu\text{m}$ fraction



probability resamples for each set of model runs) were less than 0.01, indicating that the un-mixing model was effective in estimating the true posterior densities.

For the $< 63\text{-}\mu\text{m}$ fraction, using the KW-H composite signature, the relative contributions (with corresponding 5–95% uncertainty bounds) from alluvial fans, aeolian sand dunes, and agricultural land were estimated as 98.3% (95.1–99.7%), 0.4% (0.0–1.8%), and 1.1% (0.1–4.4%), compared with 98.6% (95.8–99.6%), 0.3% (0.0–1.4%), and 0.8% (0.1–3.6%), using a composite signature selected using a combination of KW-H and DFA, or 96.2% (89.9–99.2%), 1.1% (0.1–4.5%), and 2.1% (0.2–8.3%), using a fingerprint selected using KW-H and PCCA, or 98.4% (95.2–99.6%), 0.4% (0.0–1.5%), and 1.0% (0.1–4.1%), using a fingerprint selected using KW-H and

GCRTM. The root mean square difference between the apportionments results for alluvial fans, sand dunes, and agricultural lands using the different fingerprints and using this finer particle size fraction was 1.6%, 0.5%, and 1.6%, respectively.

For the $63\text{--}125\text{-}\mu\text{m}$ fraction, using the KW-H composite signature, the respective relative contributions from alluvial fans, aeolian sand dunes, and agricultural lands were estimated as 96.6% (90.3–99.3%), 0.9% (0.1–3.4%), and 2.1% (0.2–8.5%), compared with 97.3% (92.6–99.4%), 0.8% (0.1–3.2%), and 1.5% (0.1–6.4%), using a composite signature selected using a combination of KW-H and DFA, or 88.3% (75.6–96.9%), 3.5% (0.3–12.4%), and 6.4% (0.6–20.3%), using a fingerprint selected using KW-H and PCCA, or 93.8% (83–98.7%), 1.4% (0.1–5.6%), and 3.8% (0.3–

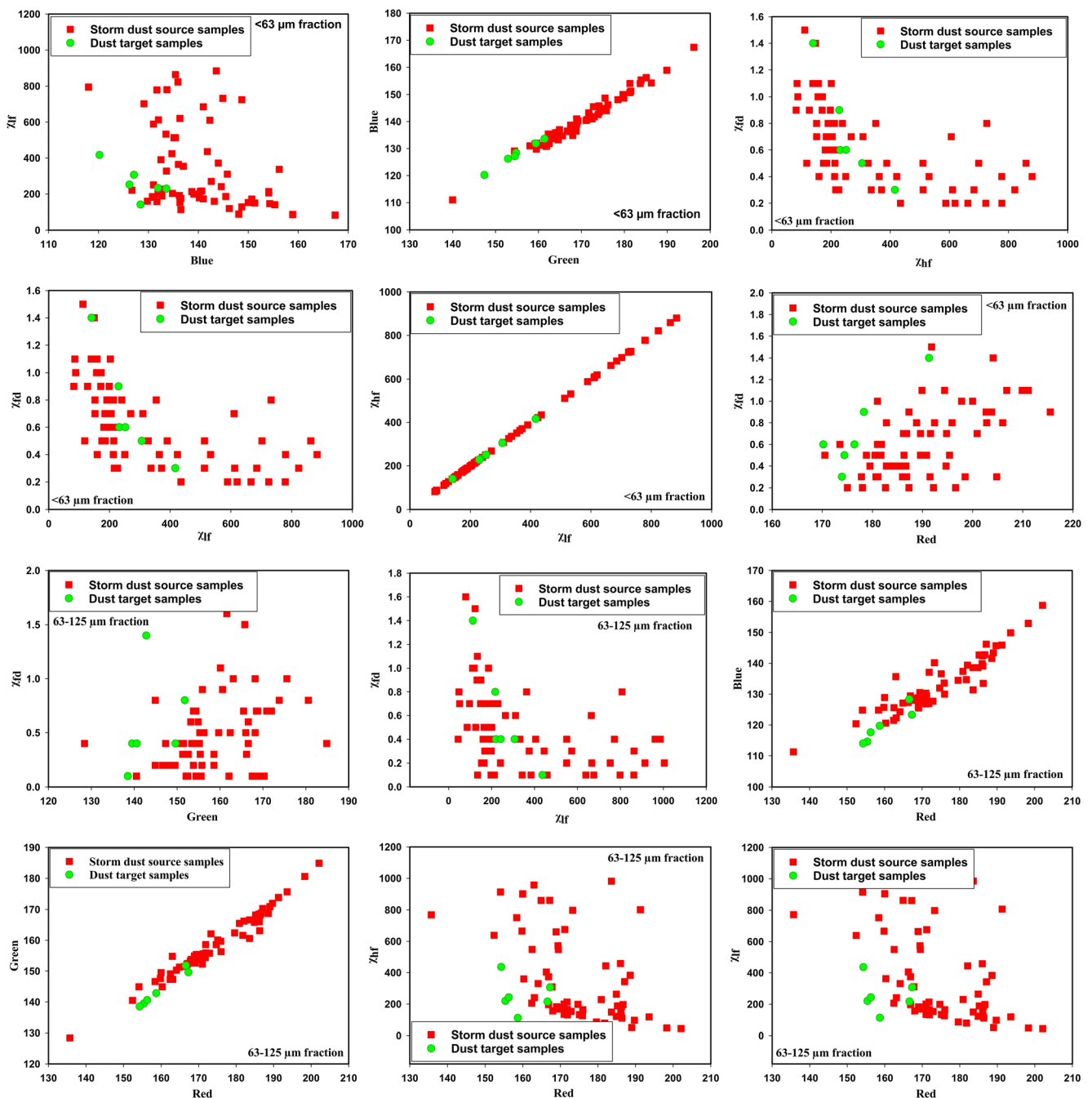


Fig. 7 Biplots of all pairings for some tracers selected in the final composite signatures for discriminating and apportioning the storm dust source contributions. Top six plots are for the < 63- μ m fraction, and the bottom six plots are for the 63–125- μ m fraction

15.3%), using a fingerprint selected using KW-H and GCRTM. The root mean square difference between the Modified MixSIR results for alluvial fans, sand dunes, and agricultural lands using the alternative fingerprints was 5.8%, 1.8%, and 3.1%, respectively. For both the < 63- and 63–125- μ m particle size fractions, all the composite signatures suggested that alluvial fans were the dominant source of the target dust samples (the overall mean contributions from this source using the different composite signatures were estimated at 97.9% and 94%, respectively).

Pairwise comparisons of the distributions of the posterior proportional contributions predicted for the three dust end members using the four different composite signatures for both particle size fractions are presented in Table 6. The Z statistic in the Wald-Wolfowitz runs test is affected by sample size and the biggest absolute difference between the two distributions being compared. A significance value of < 0.05 shows that the two distributions are significantly different. Accordingly, the results of Wald-Wolfowitz runs test pairwise comparisons indicated that most of the comparisons were significantly different (Table 6).

Table 6 Wald-Wolfowitz runs test pairwise comparisons of the probability density functions computed for the predicted contributions from dust sources based on composite signatures selected by different statistical approaches

Paired statistical approaches in selecting tracers	Statistics	Storm dust source contributions		
		Alluvial fan	Sand dunes	Agricultural land
< 63-μm fraction				
KW-H test vs. combination of KW-H test and DFA	Z	0.86	0.58	0.39
	p-level	0.39	0.56	0.70
KW-H test vs. combination of KW-H test and PCCA	Z	9.51	6.65	3.69
	p-level	< 0.001	< 0.001	< 0.001
KW-H test vs. combination of KW-H test and GCRTM	Z	1.82	2.24	2.85
	p-level	0.069	0.025	0.004
Combination of KW-H test and DFA vs. combination of KW-H test and PCCA	Z	12.43	9.26	6.20
	p-level	< 0.001	< 0.001	< 0.001
Combination of KW-H test and DFA vs. combination of KW-H test and GCRTM	Z	0.76	1.39	0.65
	p-level	0.45	0.16	0.52
Combination of KW-H test and PCCA vs. combination of KW-H test and GCRTM	Z	10.80	8.65	4.73
	p-level	< 0.001	< 0.001	< 0.001
63–125-μm fraction				
KW-H test vs. combination of KW-H test and DFA	Z	1.9	1.8	3.2
	p-level	0.063	0.078	0.001
KW-H test vs. combination of KW-H test and PCCA	Z	20.9	14.2	10.0
	p-level	< 0.001	< 0.001	< 0.001
KW-H test vs. combination of KW-H test and GCRTM	Z	4.1	1.6	3.1
	p-level	< 0.001	0.1	0.002
Combination of KW-H test and DFA vs. combination of KW-H test and PCCA	Z	24.6	13.9	13.7
	p-level	< 0.001	< 0.001	< 0.001
Combination of KW-H test and DFA vs. combination of KW-H test and GCRTM	Z	7.8	2.6	5.0
	p-level	< 0.001	0.008	< 0.001
Combination of KW-H test and PCCA vs. combination of KW-H test and GCRTM	Z	6.8	5.3	0.03
	p-level	< 0.001	< 0.001	1.0

For the < 63- μ m fraction, 7 from a total of 18 possible pairwise comparisons of the source proportions predicted using the different composite signatures were not significantly different (Table 6). For the 63–125- μ m fraction, only 4 from 18 possible pairwise comparisons were not significantly different (Table 6).

For the < 63- μ m fraction (Table 7), the RMSE and MAE estimates based on the virtual mixture tests for the different final composite signatures ranged between 1.5–23.4% (with a corresponding mean value of 9.4%) and 1.2–20.1% (with a corresponding mean value of 8.3%), respectively. For the coarser particle size fraction (Table 8), the respective estimates ranged between 3.2–21.8% (with a mean value of 11%) and 2.8–18.8% (with a mean value of 9.8%). The mixture tests therefore suggested that the Modified MixSIR solutions for storm dust source contributions were acceptable in terms of accuracy.

At the outset of this study, it was assumed that the aeolian deposits (sand dunes) were the main source of storm dust in Bahadoran Village because of their close proximity and alignment with the dominant wind direction (Figs. 1 and 2c

and d). However, all four alternative composite signatures suggested that alluvial fans were the prevailing source of the target storm dust samples retrieved from the field. Our results are consistent with those reported by Washington et al. (2003) who, using remote sensing, reported that at regional scale in southwest Asia, alluvial fans and ephemeral lakes are important dust sources. Two particle size fractions were used in this study and here it is important to recognise that the interaction between particle size and wind velocity can govern particle transportation. More specifically, both the distance travelled and the transportation process can be influenced by the interplay between particle size and wind velocity (Pye 1987). Very fine sand (63–125 μ m) particles are typically transported shorter distances by saltation, whereas silt and clay particles (< 63 μ m) are transported longer distances. Wind conditions can interplay here since particles are transported further when the wind velocity exceeds 16 m/s. Extreme wind velocities result in the particle sizes in storm dust ranging from \leq 60 μ m (dust) to 60–2000

Table 7 Comparison of the predicted and known relative contributions from the sources to the virtual dust mixtures using the composite signatures selected by different statistical approaches and the corresponding root mean squared error (RMSE) and mean absolute error (MAE) for the < 63- μm fraction

Statistical approaches for selecting composite fingerprints	Known dust source proportions ¹			Predicted dust source proportions			RMSE	MAE
	1	2	3	1	2	3		
KW-H (tracers: red, green, blue, χ_{lf} , χ_{hf} , χ_{fd}) ²	33.3	33.3	33.3	27.6	25.9	45.4	8.8	8.4
	50	25	25	37.7	25.8	35.5	9.3	7.9
	25	50	25	19.2	48.5	30.5	4.7	4.3
	25	25	50	22.5	26.3	49.9	1.6	1.3
	75	10	15	52.3	13.8	32.7	16.8	14.7
	15	75	10	10.5	68.2	19.6	7.3	7.0
	10	15	75	11.3	19.1	67.7	4.9	4.2
Combination of KW-H and DFA (tracers: red, green, blue, χ_{fd})	33.3	33.3	33.3	36.8	25	37.7	5.8	5.4
	50	25	25	41.4	25.3	32.9	6.7	5.6
	25	50	25	25.9	47.4	25.1	1.6	1.2
	25	25	50	35	25.8	38.7	8.7	7.4
	75	10	15	52.3	13.4	33.2	16.9	14.8
	15	75	10	14	68.3	14.9	4.8	4.2
	10	15	75	31.2	17.5	50.6	18.7	16.0
Combination of KW-H and PCCA (tracers: red, χ_{hf})	33.3	33.3	33.3	29.6	23.7	42.7	8.0	7.6
	50	25	25	37.7	23.2	35	9.2	8.0
	25	50	25	19.2	42.3	34.1	7.7	7.5
	25	25	50	24.6	27.6	44.1	3.7	3.0
	75	10	15	51.6	14.4	30.3	16.3	14.4
	15	75	10	11	59.9	25	12.5	11.4
	10	15	75	18.5	24.3	53.5	14.4	13.1
Combination of KW-H and GCRTM (tracers: red, green, blue)	33.3	33.3	33.3	36	24.1	39	6.4	5.9
	50	25	25	36.5	24.8	37.9	10.8	8.9
	25	50	25	24.3	47.6	25.9	1.5	1.3
	25	25	50	33.8	24.5	40.5	7.5	6.3
	75	10	15	44.5	13.2	41.5	23.4	20.1
	15	75	10	13.8	68.3	14.5	4.7	4.1
	10	15	75	35	16.5	47.5	21.5	18.0

¹ Dust sources comprising the following: 1, alluvial fan; 2, sand dunes; and 3, agricultural land

² Magnetic susceptibility at low frequency (χ_{lf}) and high frequency (χ_{hf}) and dependent frequency (χ_{fd})

μm (sand) (Shao 2008). In our study area, the dominance of the alluvial fan source reflects the interplay between prevailing wind velocities and the sparse vegetation cover on the alluvial fans (Fig. 2a and b). Land surface characteristics play an important role in the opportunity for dust mobilisation and the particle size characteristics of storm dust. Observational evidence for the alluvial fans in the study area, including the appearance of gravel and stones on the land surface, lack of soil moisture, and stone pavements, supported the finding that alluvial fans are an important source of the sampled storm dust. Dust storms in the Bahadoran region started ~ 10 years ago due to decreasing soil moisture and vegetation cover due to anthropogenic activities and reduced rainfall. Climate change and drought

have intensified the aridity thereby increasing the supply of dust at risk of remobilisation by wind.

To date, studies investigating storm dust provenance have used a range of approaches including remote sensing, as well as sedimentological or meteorological (synoptic) approaches to infer the sources of storm dust. For example, Al-Hemoud et al. (2020) used satellite images to suggest that storm dust in Kuwait is sourced from a wind erosion hot spot in southern Iraq. Achilleos et al. (2020) reported that an intense dust event in 2006 (24 h- PM_{10}) in the Eastern Mediterranean originated from the Sahara desert. Farahani and Arhami (2020) argued that Iraqi and Syrian deserts contributed ~ 40% of the particulate matter (PM) in Tehran during dust storms. In our study, rather than infer the sources of storm dust, we applied a source

Table 8 Comparison of the predicted and known relative contributions from the sources to the virtual dust mixtures using the composite signatures selected by different statistical approaches and the corresponding root mean squared error (RMSE) and mean absolute error (MAE) for the 63–125- μm fraction

Statistical approaches for selecting composite fingerprints	Known dust source proportions ¹			Predicted dust source proportions			RMSE	MAE
	1	2	3	1	2	3		
KW-H (tracers: red, green, blue, χ_{lf} , χ_{hf} , χ_{fd}) ²	33.3	33.3	33.3	26.3	24.2	47.9	10.7	10.2
	50	25	25	34.8	24.1	39.2	12.0	10.1
	25	50	25	17.4	45.4	35.6	8.0	7.6
	25	25	50	20.2	27.4	51.1	3.2	2.8
	75	10	15	50.2	14.5	32.5	17.7	15.6
	15	75	10	10.1	62.1	25.8	12.1	11.2
	10	15	75	10.9	21.8	65.6	6.7	5.7
Combination of KW-H and DFA (tracers: red, green, blue, χ_{fd})	33.3	33.3	33.3	33.7	24.1	39.8	6.5	5.4
	50	25	25	35.5	23.2	39.3	11.8	10.2
	25	50	25	21.5	44.8	30.7	4.9	4.8
	25	25	50	28.4	27.7	41.8	5.4	4.8
	75	10	15	49.2	13.2	34.5	18.8	16.2
	15	75	10	14.2	62.5	19.8	9.2	7.7
	10	15	75	25.9	23.1	49	18.2	16.7
Combination of KW-H and PCCA (tracers: red, χ_{hf})	33.3	33.3	33.3	28.4	26.6	39.3	5.9	5.9
	50	25	25	36.2	24.7	33.4	9.3	7.5
	25	50	25	18.7	38.1	38.3	10.9	10.5
	25	25	50	22.4	30.7	41.2	6.2	5.7
	75	10	15	49.8	17.4	26.8	16.6	14.8
	15	75	10	11.8	47.5	35.7	21.8	18.8
	10	15	75	15.7	32.2	47	19.3	17.0
Combination of KW-H and GCRTM (tracers: red, green, χ_{lf} , χ_{hf} , χ_{fd})	33.3	33.3	33.3	27.3	26.2	43.9	8.1	7.9
	50	25	25	36	26	35.2	10.0	8.4
	25	50	25	17.6	43.7	36.4	8.6	8.4
	25	25	50	20.8	30.5	46.6	4.5	4.4
	75	10	15	51.8	16.9	27.4	15.7	14.2
	15	75	10	10.3	58	29.5	15.2	13.7
	10	15	75	11.3	27.2	59.4	11.5	9.7

¹ Dust sources comprising the following: 1, alluvial fan; 2, sand dunes; and 3, agricultural land

² Magnetic susceptibility at low frequency (χ_{lf}) and high frequency (χ_{hf}) and dependent frequency (χ_{fd})

fingerprinting approach with explicit estimation of uncertainty for the predicted source proportions. The results are promising and suggest that wider applications could be as equally successful. Reliable data on the provenance of storm dust is needed to target remedial actions.

Limitations of the work

The storm dust tracing results from our work must be interpreted in the knowledge of some limitations and uncertainties. Compared with fluvial sediment source fingerprinting, storm dust tracing is more complex. In the case of catchment scale fluvial sediment tracing, when we collect target

sediment samples (e.g. suspended, channel bed sediment), we are more certain that all particles have originated from the upstream catchment and not from neighbouring catchments. In dust tracing, however, storm dust origin is strongly affected by wind direction and prevailing meteorological conditions. Air masses can cover large scales including up to regional or continental and this can raise challenges for delineation of known sources. In the case of our study reported here, both field survey and questionnaires were used to assess potential storm dust sources. Local resident questionnaires can help to evaluate the history of local dust storms.

Dust sample collection during storm events is another challenge: there are two main kinds of dust comprising infusing

(downfall) dust with vertical movement and stream (moving or flow) dust with lateral movement. In order to trap both dust types, both a siphon dust collector and marble dust sampler were used. In the siphon dust collector, it is necessary to embed a fine filter to have sufficient capacity for trapping finer dust particles. Although available budgets affect the dust sample numbers collected for any dust tracing exercise, the collection of both kinds of dust samples across an extended area and bulking these into fewer composite samples for laboratory analyses improves representativeness by considering macro-scale spatial variations in the character and properties of target storm dust. Sampling during storm events also requires consideration of the temporal dimension. In the study reported herein, to improve robustness, dust samples were collected from more than one site and one height to explore any potential scale-dependency associated with dust tracers during transportation from the sampled sources to the target destination for sampling the dust sediment. However, here it should be borne in mind that in our study, target dust samples for source apportionment were collected from samplers that were installed at a maximum height of 4 m. We, therefore, did not sample all transported storm dust particles. Even though tracer properties were tested using the standard conservation tests currently used in source fingerprinting studies, these tests assume that any tracer property change during detachment and transportation was not sufficiently significant to impact on the predicted source proportions. Further work is needed to investigate and compare the efficiency of different types of tracers for discriminating and apportioning dust sources. Here, although there are no fixed combinations of statistical tests for selecting final composite signatures, there remains a need to explore the sensitivity of predicted source apportionment to the use of different composite signatures.

Conclusions

Applications of fingerprinting methods to assess the sources of storm dust are only just beginning to emerge in the international literature, against the context of the many more and rapidly growing numbers of applications for estimating sources of fluvial sediment. The work presented herein suggests that colour and magnetic susceptibility tracers offer low-cost options for discriminating and apportioning storm dust sources. Such composite signatures need to be applied to alternative settings to confirm this conclusion from our study. The findings from the work reported herein provide some much needed information for targeting wind erosion control measures to help protect the rural and urban receptors receiving damaging storm dust.

Funding information This study was financially supported by the Iran National Science Foundation (INSF) (grant numbers 98006889). This

project was also funded by a grant (grant number 600.4452) from the research council of Shahid Beheshti University, Tehran, Iran. ALC was supported by strategic funding from the UKRI (UK Research and Innovation) Biotechnology and Biological Sciences Research Council (BBSRC grant BBS/E/C/00010330; Soil to Nutrition project 3). SP was supported by funding from the Environment Agency (grant award 19936 awarded to ALC). ED, AK, and QC were funded to work at Rothamsted Research by the ERASMUS programme.

References

- Achilleos S et al (2020) Spatio-temporal variability of desert dust storms in Eastern Mediterranean (Crete, Cyprus, Israel) between 2006 and 2017 using a uniform methodology. *Sci Total Environ* 714:136693
- Al-Hemoud A, Al-Dousari A, Misak R, Al-Sudairawi M, Naseeb A, Al-Dashti H, Al-Dousari N (2019) Economic impact and risk assessment of sand and dust storms (SDS) on the oil and gas industry in Kuwait. *Sustainability* 11:200
- Al-Hemoud A et al (2020) Sand and dust storm trajectories from Iraq Mesopotamian flood plain to Kuwait. *Sci Total Environ* 710:136291
- Asgari N, Ayoubi S, Demattè JA (2018) Soil drainage assessment by magnetic susceptibility measures in western Iran. *Geoderma Reg* 13:35–42
- Behrooz RD, Gholami H, Telfer MW, Jansen JD, Fathabadi A (2019) Using GLUE to pull apart the provenance of atmospheric dust. *Aeolian Res* 37:1–13
- Bourliva A, Kantiranis N, Papadopoulou L, Aidona E, Christophoridis C, Kollias P, Evgenakis M, Fytianos K (2018) Seasonal and spatial variations of magnetic susceptibility and potentially toxic elements (PTEs) in road dusts of Thessaloniki city, Greece: a one-year monitoring period. *Sci Total Environ* 639:417–427
- Caitcheon GG (1993) Applying environmental magnetism to sediment tracing IAHS PUBLICATION, pp 285–285
- Collins A, Zhang Y, McChesney D, Walling D, Haley S, Smith P (2012) Sediment source tracing in a lowland agricultural catchment in southern England using a modified procedure combining statistical analysis and numerical modelling. *Sci Total Environ* 414:301–317
- Collins A, Pulley S, Foster ID, Gellis A, Porto P, Horowitz A (2017) Sediment source fingerprinting as an aid to catchment management: a review of the current state of knowledge and a methodological decision-tree for end-users. *J Environ Manag* 194:86–108
- Dearing JA, Hay KL, Baban SM, Huddleston AS, Wellington EM, Loveland P (1996) Magnetic susceptibility of soil: an evaluation of conflicting theories using a national data set. *Geophys J Int* 127: 728–734
- Farahani VJ, Arhami M (2020) Contribution of Iraqi and Syrian dust storms on particulate matter concentration during a dust storm episode in receptor cities: case study of Tehran. *Atmos Environ* 222: 117163
- Foster ID, Lees JA (2000) Tracers in geomorphology: theory and applications in tracing fine particulate sediments. In: Foster IID (ed) *Tracers in geomorphology*. J. Wiley & Sons, Chichester, pp 3–20
- Gholami H, Middleton N, Samani AAN, Wasson R (2017) Determining contribution of sand dune potential sources using radionuclides, trace and major elements in central Iran. *Arab J Geosci* 10:163
- Gholami H, Kordestani MD, Li J, Telfer MW, Fathabadi A (2019a) Diverse sources of aeolian sediment revealed in an arid landscape in southeastern Iran using a modified Bayesian un-mixing model. *Aeolian Res* 41:100547
- Gholami H, TakhtiNajad EJ, Collins AL, Fathabadi A (2019b) Monte Carlo fingerprinting of the terrestrial sources of different particle size fractions of coastal sediment deposits using geochemical tracers: some lessons for the user community. *Environ Sci Pollut Res* 26: 13560–13579

- Gholami H, Rahimi S, Fathabadi A, Habibi S, Collins AL (2020) Mapping the spatial sources of atmospheric dust using GLUE and Monte Carlo simulation. *Sci Total Environ* 723:138090. <https://doi.org/10.1016/j.scitotenv.2020.138090>
- Ginoux P, Prospero JM, Gill TE, Hsu NC, Zhao M (2012) Global-scale attribution of anthropogenic and natural dust sources and their emission rates based on MODIS Deep Blue aerosol products. *Rev Geophys*:50
- Karimi A, Khademi H, Ayoubi S (2013) Magnetic susceptibility and morphological characteristics of a loess–paleosol sequence in north-eastern Iran. *Catena* 101:56–60
- Karimi A, Haghnia GH, Ayoubi S, Safari T (2017) Impacts of geology and land use on magnetic susceptibility and selected heavy metals in surface soils of Mashhad plain, northeastern Iran. *J Appl Geophys* 138:127–134
- Liu B, Niu Q, Qu J, Zu R (2016) Quantifying the provenance of aeolian sediments using multiple composite fingerprints. *Aeolian Res* 22: 117–122
- Martínez-Carreras N et al (2010) The use of sediment colour measured by diffuse reflectance spectrometry to determine sediment sources: application to the Attert River catchment (Luxembourg). *J Hydrol* 382: 49–63
- Mathé V, Lévêque F (2003) High resolution magnetic survey for soil monitoring: detection of drainage and soil tillage effects. *Earth Planet Sci Lett* 212:241–251
- Middleton N (1986) Dust storms in the Middle East. *J Arid Environ* 10: 83–96
- Moore JW, Semmens BX (2008) Incorporating uncertainty and prior information into stable isotope mixing models. *Ecol Lett* 11:470–480
- Morris W, Versteeg J, Marvin C, McCarry B, Rukavina N (1994) Preliminary comparisons between magnetic susceptibility and polycyclic aromatic hydrocarbon content in sediments from Hamilton Harbour, western Lake Ontario. *Sci Total Environ* 152:153–160
- Muhs DR, Budahn JR (2019) New geochemical evidence for the origin of North America's largest dune field, the Nebraska Sand Hills, central Great Plains, USA. *Geomorphology* 332:188–212
- NAP (2005) National action programme to combat desertification and mitigate the effects of drought of Islamic Republic of Iran
- Nosrati K (2017) Ascribing soil erosion of hillslope components to river sediment yield. *J Environ Manag* 194:63–72. <https://doi.org/10.1016/j.jenvman.2016.10.011>
- Nosrati K, Collins AL (2019a) Fingerprinting the contribution of quarrying to fine-grained bed sediment in a mountainous catchment, Iran. *River Res Appl* 35:290–300. <https://doi.org/10.1002/rra.3408>
- Nosrati K, Collins AL (2019b) Investigating the importance of recreational roads as a sediment source in a mountainous catchment using a fingerprinting procedure with different multivariate statistical techniques and a Bayesian un-mixing model. *J Hydrol* 569:506–518. <https://doi.org/10.1016/j.jhydrol.2018.12.019>
- Nosrati K, Govers G, Semmens BX, Ward EJ (2014) A mixing model to incorporate uncertainty in sediment fingerprinting. *Geoderma* 217: 173–180
- Nosrati K, Collins AL, Madankan M (2018) Fingerprinting sub-basin spatial sediment sources using different multivariate statistical techniques and the Modified MixSIR model. *Catena* 164:32–43
- Nosrati K, Fathi Z, Collins AL (2019) Fingerprinting sub-basin spatial suspended sediment sources by combining geochemical tracers and weathering indices. *Environ Sci Pollut Res* 26:28401–28414. <https://doi.org/10.1007/s11356-019-06024-x>
- Palazón L, Navas A (2017) Variability in source sediment contributions by applying different statistic test for a Pyrenean catchment. *J Environ Manag* 194:42–53. <https://doi.org/10.1016/j.jenvman.2016.07.058>
- Palazón L, Latorre B, Gaspar L, Blake WH, Smith HG, Navas A (2015) Comparing catchment sediment fingerprinting procedures using an auto-evaluation approach with virtual sample mixtures. *Sci Total Environ* 532:456–466
- Prospero JM, Ginoux P, Torres O, Nicholson SE, Gill TE (2002) Environmental characterization of global sources of atmospheric soil dust identified with the Nimbus 7 Total Ozone Mapping Spectrometer (TOMS) absorbing aerosol product. *Rev Geophys* 40:2-1–2-31
- Pulley S, Foster I, Collins AL (2017) The impact of catchment source group classification on the accuracy of sediment fingerprinting outputs. *J Environ Manag* 194:16–26
- Pye K (1987) Aeolian dust and dust deposits. Academic Press, London
- Ravi S et al (2011) Aeolian processes and the biosphere. *Rev Geophys* 49
- Reheis M (2006) A 16-year record of eolian dust in Southern Nevada and California, USA: controls on dust generation and accumulation. *J Arid Environ* 67:487–520
- Shao Y (2008) Physics and modelling of wind erosion vol 37. Springer Science & Business Media
- Shao Y et al (2011) Dust cycle: an emerging core theme in Earth system science. *Aeolian Res* 2:181–204
- Shenggao L (2000) Lithological factors affecting magnetic susceptibility of subtropical soils, Zhejiang Province, China. *Catena* 40:359–373
- StatSoft (2008) STATISTICA: [data analysis software system], Version 8.0 for Windows update. StatSoft, Inc., 8.0 for Windows update edn
- Thomas D, Middleton N (1997) World atlas of desertification. Arnold
- Tiecher T, Caner L, Minella JPG, Dos Santos DR (2015) Combining visible-based-color parameters and geochemical tracers to improve sediment source discrimination and apportionment. *Sci Total Environ* 527:135–149
- Valaee M, Ayoubi S, Khormali F, Lu SG, Karimzadeh HR (2016) Using magnetic susceptibility to discriminate between soil moisture regimes in selected loess and loess-like soils in northern Iran. *J Appl Geophys* 127:23–30
- Washington R, Todd M, Middleton NJ, Goudie AS (2003) Dust-storm source areas determined by the total ozone monitoring spectrometer and surface observations. *Ann Assoc Am Geogr* 93:297–313

Publisher's note Springer Nature remains neutral with regard to jurisdictional claims in published maps and institutional affiliations.